



Research article

A parametric design framework for the mass customization of bicycle helmet



Zhaohua Zhu^a, Yi Huang^{a,*}, Wenxuan Ji^a, Jintuo Zhu^b, Wenyu Wang^a

^a School of Architecture & Design, China University of Mining and Technology, Daxue Road, Xuzhou, China

^b Research Institute of Occupational Health, China University of Mining and Technology, Daxue Road, Xuzhou, China

ARTICLE INFO

Keywords:

3D head shape clustering
K-medoids algorithm
Bicycle helmet
Mass customization design
Parametric modeling

ABSTRACT

Cluster analysis of 3D head shapes plays a crucial role in the mass customization design of products related to the head. Head shapes exhibit variations across different races, and designing helmets exclusively for Chinese individuals cannot solely rely on or reference foreign head models. Currently, research on cluster analysis of Chinese head shapes is limited, especially concerning shape variances. To address this, we developed an improved *k*-medoids algorithm and integrated Cluster Validity Index as an assessment metric. This enabled us to cluster 339 Chinese young males aged 18 to 30 into 7 groups based on their head shapes. By comparing our improved algorithm to the traditional *k*-medoids method, we affirmed its superiority in achieving higher sample participation rates and reducing inter-cluster sample disparities. To simplify the helmet design and editing process, and to improve the efficiency of mass customization, we have developed a parametric modeling program for bicycle helmets based on the head shape clustering results. Results from the Helmet Fit Index and stress simulation analysis demonstrate that our approach significantly enhances helmet fit and wearer comfort.

1. Introduction

The head is one of the most critical parts of the body, and a protective helmet is essential equipment to ensure the safety of cyclists. Previous researches have demonstrated that a properly fitting helmet should maintain an adequate and uniform gap between the head and the helmet, thereby reducing the risk of head injuries [1,2]. Ill-fitting helmets, on the other hand, significantly reduce their protective capabilities and increase the risk of head injuries [3–5]. In addition, ill-fitting helmets can decrease comfort, leading some cyclists to choose not to wear them [6]. Due to significant variations in head size and shape among different populations and even within the same population, standard helmets produced on a large scale may not accommodate all head shapes, potentially causing users to wear helmets that are either too small or too large. Therefore, conducting statistical analysis of head shapes is crucial to provide reliable data support for helmet design, ultimately improving helmet fit.

The primary objective during the design and development phase of wearable products is undoubtedly to meet the comfort requirements of the consumers. Over the past two decades, anthropometric measurements have been utilized in various industries, including ear products [7,8], clothing [9,10], head and facial products [11–13], and footwear [14,15]. However, it is essential to recognize that these limited measurements fall short in fully capturing the shape attributes of the human body, which are crucial for creating well-fitting products [16]. For instance, bicycle helmet sizes, determined by head circumference, length, and breadth, may not

* Corresponding author.

E-mail address: 1427859254@qq.com (Y. Huang).

accommodate wearer's head shape. As highlighted by Ellena et al. [17], a critical aspect of helmet fit is the snug conformity to the head shape without leaving any significant gaps between the helmet liner and the head. Advances in 3D (Three Dimensional) scanning technology, such as 3D scanners, MRI (Magnetic Resonance Imaging), and CT (Computer Tomography), have motivated researchers and manufacturers to incorporate comprehensive 3D anthropometric data in product design. These techniques provide a large set of data points that offer in-depth information about the shape characteristics of the scanned head [18]. In recent years, a multitude of researchers have been exploring the utilization of 3D head and face scans from individuals of diverse ethnicities to design customized head and face-related products. These scans undergo processing and modelling using a combination of CAD (Computer Aided Design) software and RE (reverse engineering) techniques, resulting in editable 3D models that can be employed in the creation of personalized helmets [19], eyeglasses [20], cosmetic masks [21,22], and eye massagers [23]. Research conducted by Zhang et al. [24,25] even developed an algorithm predicting 3D head shape directly from incomplete scans, further enhancing the customization process for personal helmets. Bake and Lee [26,27] underscores the importance of considering an individual's overall 3D body attributes when designing these products, leading to better fitting and more comfortable outcomes compared to designs based solely on size. The objective of customization is to meet the specific needs of individual users. While products tailored to perfectly fit a customer's body shape offer excellent comfort, custom-designed products can be expensive and time-consuming to produce. Mass customization, on the other hand, aims to provide customized products or services to consumers on a large scale at a cost that is reasonable compared to traditional customization processes. Striking a balance between achieving an ideal fit for the majority of users and ensuring production convenience has become a focal point for many researchers. This focus has led to the development of various size and shape systems for wearable products based on anthropometric data derived from population samples [28]. For example, Ellena et al. [29] utilized a non-rigid point set registration algorithm to extract 13,000 points representing head protection areas from 190 scanned head models of the Australian population. Using this data, they applied an improved hierarchical clustering algorithm with a clustering threshold of 20 mm and considered optimal clustering evaluation criteria to categorize head shapes into four clusters. Subsequently, they designed bicycle helmet liners based on the average shape of these clusters and assessed the stability, comfort, and fit of the helmet liners through dynamic stability tests and a Helmet Fit Index, which took into account standoff distance, gap uniformity, and head protection ratio [17,29,30]. In another approach, Lacko et al. [31] and Verwulgen et al. [32] classified 100 head surfaces obtained from MRI (Magnetic Resonance Imaging) scans into three categories by considering the entire head's geometry. They calculated the cluster medoid for each category, which served as the reference model for creating mass-customized brain computer interface headsets. Similarly, Bai et al. [33] developed a parametric product design framework for mass-customized eyewear products accessible via a web platform. This framework involved creating a 3D face model based on a series of measurable and adjustable parameters related to facial geometry.

Numerous prior studies have observed significant variations in head shape among individuals from diverse nations and ethnic backgrounds [2,34–36]. Ball et al. [4] involved anthropometric statistical analysis and shape comparisons, which emphasized that Chinese heads typically feature a rounder shape compared to Western heads. They also identified distinctive characteristics such as a flatter back and forehead. Based on these findings, it was concluded that head-related products designed for Western head templates may not be suitable for Chinese individuals. The implementation of a proposed regulation mandating helmet usage for all drivers by the Traffic Administration of China's Ministry of Public Security, aimed at enhancing the safety of motorcyclists, has led to a significant surge in the demand for helmets in the Chinese market.

Obtaining detailed information about the normal head shape of the Chinese population is of paramount importance for the ergonomic design of head-related products. To the best of our knowledge, there are few studies that approach the analysis of Chinese head shapes from the perspective of shape differences, as opposed to relying solely on limited head feature dimensions. Therefore, we have developed an improved head shape clustering algorithm to systematically analyze the variations in head shapes among the Chinese population, providing a foundation for the design of mass-customized bicycle helmets with enhanced fit and comfort. The main contributions are summarized as follows.

- We developed a technique for reconstructing head shapes with minimal reconstruction errors. This was achieved by converting all head meshes acquired from 3D scans, which consist of varying quantities of point clouds, into Non-Uniform Rational B-Spline (NURBS) surfaces with an identical number of vertices while maintaining consistent indices and meanings. These NURBS surfaces served as the foundational data for head shape clustering.
- We developed an improved k -medoids algorithm tailored for head shape clustering. In comparison to traditional algorithms, the improved algorithm offers the advantage of ensuring minimal intra-cluster sample dissimilarity, significant inter-cluster sample dissimilarity, and a high participation rate of samples in the clustering process. Additionally, we determined the optimal number of clustering clusters using the Cluster Validity Index (CVI) and Helmet Fit Index (HFI).
- We constructed a parametric modelling program for designing bicycle helmets using Grasshopper software, aiming to assist designers in enhancing the efficiency of mass-customized helmet design.

2. Methods

To realize the mass customization technology for designing bicycle helmet products based on head shape clustering, an extensive collection of 3D head models is initially required. Subsequently, these gathered head models need to be reconstructed within a standardized coordinate system to possess identical topology and an equal number of vertices (with corresponding indices and meanings). Following this, an improved clustering algorithm is employed for the analysis and comparison of head shapes. The fundamental workflow for clustering 3D head shapes and facilitating the mass customization of helmet designs includes (see Fig. 1): (1)

Collection of 3D head models (see Section 2.1), (2) Preprocessing and alignment of 3D head models (see Section 2.2), (3) Extraction and reconstruction of head protection areas (see Section 2.3), (4) 3D head shape clustering (see Section 2.4), and (5) Designing mass-customized bicycle helmets and validating fit and wearing comfort (see Sections 2.5).

2.1. Collection of 3D head models

A total of 339 young Chinese males aged 18–30 years were recruited for this study, with an average age of 20.4 ± 2.3 years. Individuals with a history of craniofacial trauma, congenital anomalies, or prior surgery were excluded from the study. Head scans were conducted using a HandScan300 3D scanner (CREAFORM Inc., Lévis, Quebec, Canada) with a precision of 0.04 mm and processed with VX-elements software, as illustrated in Fig. 2(a) and(b). To minimize surface irregularities and accurately capture the head shape, all participants wore seamless swimming caps pressed against their hair. Ethical approval was obtained from the institutional ethics committee prior to the study, and all participants provided written informed consent after receiving detailed information about the experiment and their rights.

2.2. Preprocessing and alignment of 3D head models

The preprocessing of the 3D scanned head models was conducted using Geomagic Wrap 2017 (3D Systems Inc., USA). As shown in Fig. 3(a), the Mesh Doctor tool was employed to effectively eliminate spikes and bumps present in the scanned images. Subsequently, the Fill Holes tool was utilized to repair any missing sections within the mesh (see Fig. 3(b)). Additionally, the Smooth tool was applied to enhance the mesh quality by reducing the angles between individual polygons, resulting in a smoother representation (see Fig. 3(c)).

In the clustering process, accurately calculating the distances between corresponding data points in a unified coordinate system is crucial for evaluating the similarity between head models. However, this task may be challenging due to variations in the number of point clouds and different positions and orientations of 3D head models, stemming from different head poses adopted during the scanning process. To address this issue, an alignment procedure was developed to standardize the position and orientation of the head meshes. This procedure involves creating three planes for each head model: the Sagittal plane, Horizontal plane, and Coronal plane, as shown in Fig. 4(a). The Sagittal plane is symmetrically established with respect to the head. The Horizontal plane is established by utilizing points on the tragus and the outer corners of the eye sockets. The Coronal plane is perpendicular to the sagittal and horizontal planes, with its position determined by the ear tragus points. Finally, these three planes are used to create an orthogonal coordinate system, aligned with the standard coordinate system in Geomagic Design X software (3D Systems Inc., USA). The head modes of different samples after alignment are shown in Fig. 4(b).

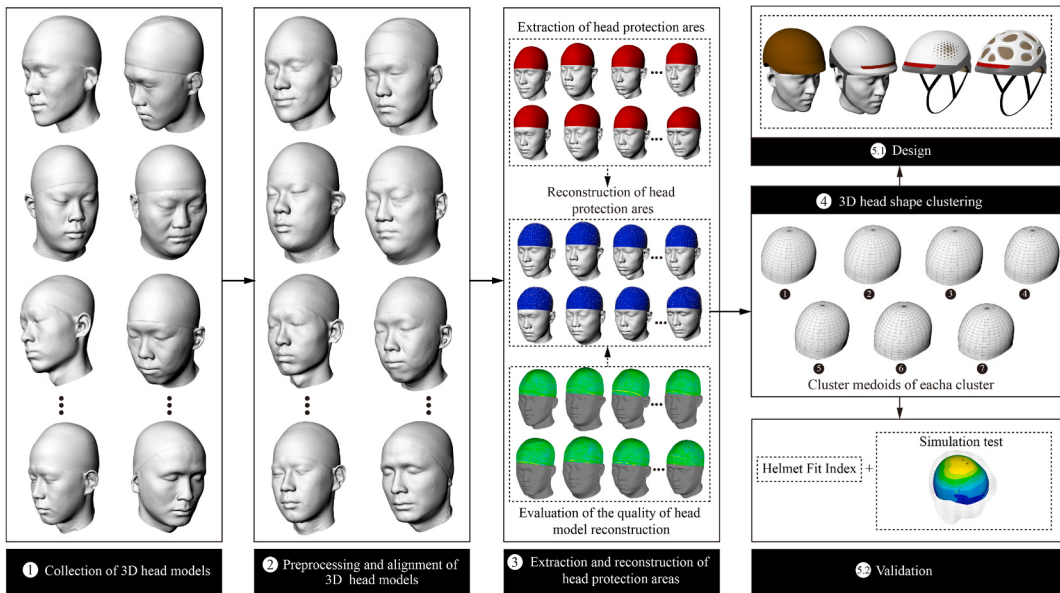


Fig. 1. The main workflow for 3D head shape clustering and mass customization design includes the following steps: (1) Collection of 3D head models (see Section 2.1), (2) Preprocessing and alignment of 3D head models (see Section 2.2), (3) Extraction and reconstruction of head protection areas (the method for extracting and reconstructing head protection areas is described in Section 2.3, and the analysis of reconstruction results is presented in Section 3.1), (4) 3D head shape clustering (the process of the improved k-medoids clustering algorithm is detailed in Section 2.4, and the results and analysis of head shape clustering are discussed in Section 3.2), (5) Design and validation (the methods for design validation are presented in Section 2.5, while the results can be found in Section 4).

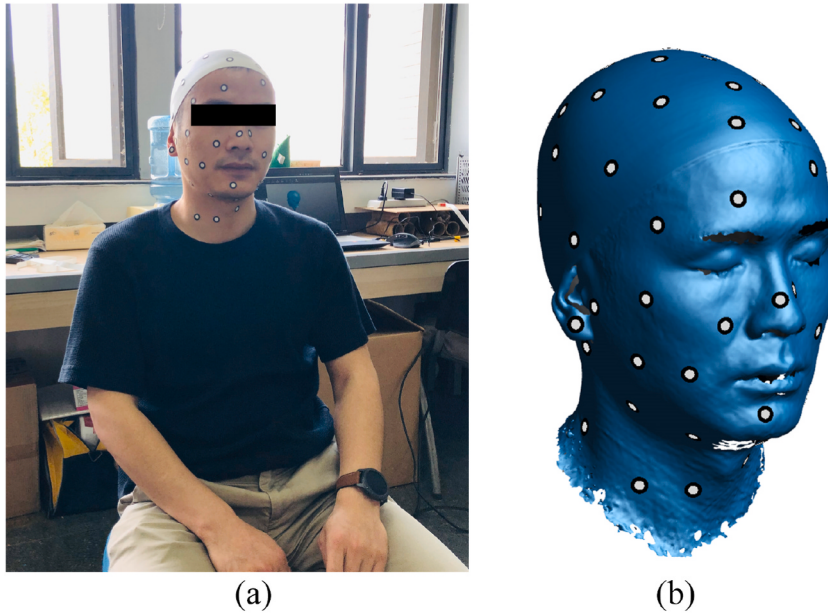


Fig. 2. 3D head models scan. (a) Pasting of positioning markers. (b) Scanned 3D head model.

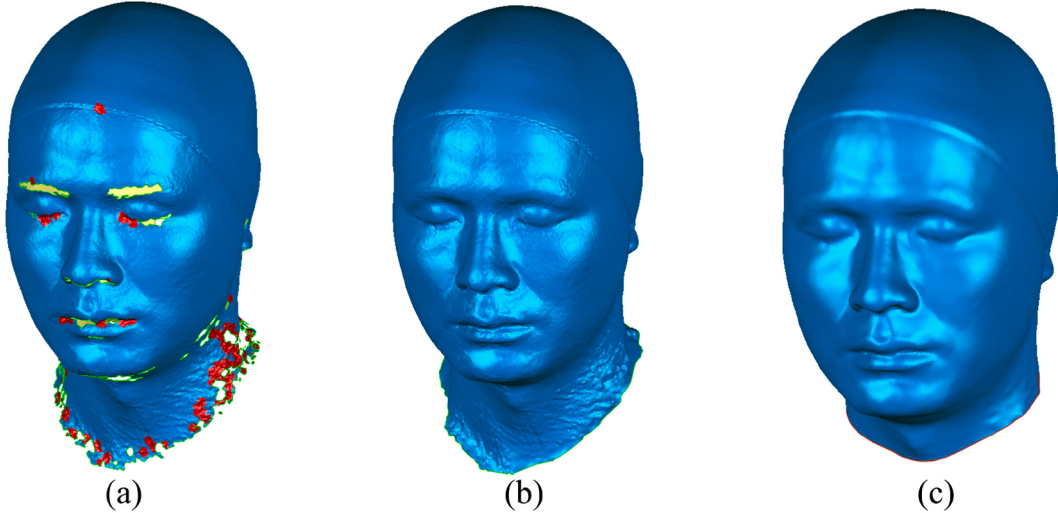


Fig. 3. Preprocessing of the 3D scanned head mesh. (a) Eliminate the spikes and bumps. (b) Repair the missing parts. (c) Smooth the mesh.

2.3. Extraction and reconstruction of head protection areas

In accordance with GB811-2022 [37], the protective area of a bicycle helmet is defined as the region above plane A in Fig. 5. The calculation of this area is achieved by determining the distance between the horizontal plane and plane A. The value of distance X is determined by the head circumference of each sample. When the head circumference falls within the range of 540–560 mm, the value of distance X is 25 mm. When the head circumference is between 560 and 580 mm, the value of distance X is 27 mm. And when the head circumference falls within the range of 580–600 mm, the value of distance X is 29 mm.

To carry out a clustering analysis of head shape, the same number and type of head data points were extracted from each 3D model. This was achieved by reconstructing all of the 3D head models as surfaces with the same topology. The steps involved in the data point extraction and surface reconstruction are described below.

- (1) Trim the Sagittal plane of each model using the Coronal and Horizontal planes, then array these trimmed Sagittal planes to obtain n surfaces intersecting the head protection area (as shown in Fig. 6 (a) and (b));

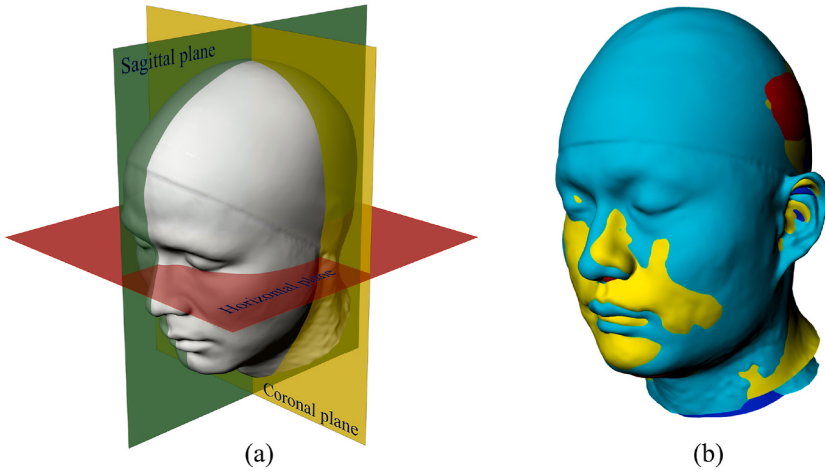


Fig. 4. Head alignment. (a) Establishment of the Sagittal, Horizontal, and Coronal planes. (b) Aligned head models of different samples.

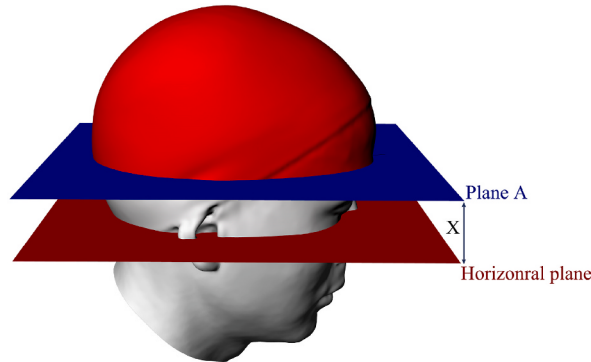


Fig. 5. Determination of the head protection area of the bicycle helmet.

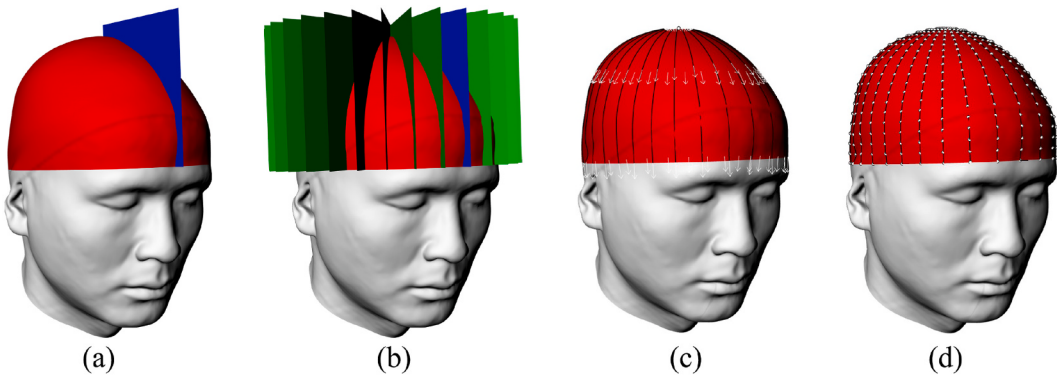


Fig. 6. Extracting the data points of head from the 3D head model. (a) and (b) Trim and array Sagittal plane. (c) Unify the normal direction of intersecting curves. (d) Reconstruct intersecting curves and extract data points.

- (2) Calculate and extract the intersecting curves between the head protection area and the arrayed surfaces, and adjust the normal direction of these curves so that they all start from the top of the head and end at the edge of the head protection area (as shown in Fig. 6(c));
- (3) Number and sort the intersecting curves, and sequentially reconstruct them as first-order curves with N points (as depicted in Fig. 6(d)), ensuring that the maximum deviation between the reconstructed curves and original curves is less than 0.01 mm. Then, save the 3D coordinate values of $n \times N$ data points in a txt file.

To perform clustering analysis of head shapes, steps (2) and (3) in the data point extraction and surface reconstruction process were implemented in a specific manner. This involved ensuring that the normal direction of intersecting curves was consistent and generating the curves in a predefined order to arrange the 3D coordinates of the data points extracted from each sample in a consistent sequence from 1 to $n \times N$. This standardized arrangement made it easier for the related programs to read and compare the coordinate values of corresponding points between the samples, line by line, during the clustering process. Without this method, it would have been challenging for the program to accurately assess the similarities between the samples.

2.4. 3D head shape clustering

2.4.1. Traditional k -medoids algorithm

Clustering is a technique that involves grouping data based on similar characteristics into clusters. Usually, the average Euclidean distance between corresponding points on two individual head surfaces is employed to facilitate the shape clustering process. The k -medoids clustering algorithm is a variant of k -means clustering, relying on the distance to the cluster medoids instead of cluster means [18]. This algorithm is widely used in data mining and clustering. If a total of S samples were scanned for clustering, where $S = \{s_1, s_2, \dots, s_n\}$, the fundamental steps of the k -medoids clustering algorithm are as follows:

- (1) Set the number of clusters as K .
- (2) Randomly select K initial cluster medoids from S , $m_1, m_2, \dots, m_K \in S$.
- (3) Take $s \in S$, if $d(s, m_j) \leq d(s, m_i)$, $i \neq j$, $j \in (1, 2, \dots, K)$, $i \in (1, 2, \dots, K)$, assign s to cluster K_j .
- (4) If $m' \in K_i$, $\sum_{s \in K_i} d(m', s)$ is minimal, replace m_i with m' as the new cluster medoids of cluster K_i .
- (5) Repeat steps (3)–(4) until the cluster medoids remains constant or the cost function is minimal.

2.4.2. Improved k -medoids algorithm

The notion that a sample having the smallest total distance to a cluster medoid implies high similarity between the sample and the medoid can be misleading. This is because, when the distribution of distances between the sample and the medoid is uneven, even if the overall distance sum is small, there may still be significant local disparities. To ensure accurate clustering, it is essential to establish a high degree of similarity among the samples within a single cluster based on head shape while maintaining dissimilarity among samples in different clusters. To overcome the limitations of traditional k -medoids algorithms, this study introduces an improved k -medoids algorithm for head shape classification. This new algorithm is based on an approach similar to the one used by Lacko et al. [31], and its steps are outlined as follows.

- (1) Set the number of clusters as K and the distance threshold value between the corresponding data points of the samples and the cluster medoids as D .
- (2) Randomly select K initial cluster medoids from S , $m_1, m_2, \dots, m_K \in S$.
- (3) Take $s \in S$, if $d(s, m_j) \leq d(s, m_i)$, $i \neq j$, $j \in (1, 2, \dots, K)$, $i \in (1, 2, \dots, K)$, the distances between the corresponding data points of the sample s and cluster medoid m_j are all less than D , and the intersection of $\text{box}(K_j \cup \{s\})$ with $\text{box}(K_i)$ is void, then assign s to K_j .
- (4) If the intersection of $\text{box}(K_j \cup \{s\})$ with $\text{box}(K_i)$ is non-void, calculate the intersection of $\text{box}(K_l \cup \{s\})$ with $\text{box}(K_i)$, $i \neq l \in (1, 2, \dots, K)$:

If the intersection of $\text{box}(K_l \cup \{s\})$ with $\text{box}(K_i)$ is void, select l , $d(s, m_l) \leq d(s, m_i)$, then add s to cluster K_l ;
If the intersection of $\text{box}(K_l \cup \{s\})$ with $\text{box}(K_i)$ is non-void, label s as outlier.

- (5) If $m' \in K_i$, $\sum_{s \in K_i} d(m', s)$ is minimal, replace m_i with m' as the new cluster medoid of cluster K_i .
- (6) Repeat steps (3)–(5) until the cluster medoids remains constant or the cost function is minimal.

Additionally, we evaluate the quality of clustering and identify the optimal number of clusters through the utilization of the Cluster Validity Index (CVI) [31,38]. The calculation procedure for CVI is elaborated in equations (1)–(3).

$$\text{intra} = \frac{1}{N} \sum_{c=1}^K \sum_{i=1}^{n_s^c} \|s_i^c - m^c\| \quad (1)$$

$$\text{inter} = \frac{1}{K(K-1)} \sum_{c=1}^{K-1} \sum_{i=c+1}^{n_s^c} \|m^c - m'^c\| \quad (2)$$

$$\text{CVI} = \frac{\text{intra}}{\text{inter}} \quad (3)$$

Where, intra represents the mean of the sum of distances from all samples within a cluster to its cluster medoid, while inter represents the mean of distances between cluster medoids of different clusters. A smaller intra and a larger inter indicate higher clustering quality

(lower CVI value). K denotes the number of clusters, N is the total number of samples, s^c represents the sample set of cluster c , n_s^c is the number of samples in cluster c , and m^c is the cluster center of cluster c .

2.5. Evaluation of fit and wearing comfort for bicycle helmet

2.5.1. Evaluation of fit by Helmet Fit Index

Ellena et al. [17,29] developed a method known as the Helmet Fit Index (HFI) to quantitatively evaluate the fit between helmet liners and human head shapes. This approach combines 3D anthropometric data with computational tools, enabling researchers to examine the consistency between a specific helmet model and the entire head surface covered by the helmet. By incorporating Standoff Distance (SOD) and Gap Uniformity (GU), the HFI can calculate a fit score for a given helmet and individual head, ranging from 0 (indicating an extremely poor fit) to 100 (indicating a perfect fit). The calculation procedure for HFI is elaborated in equation (4).

$$\text{HFI} = \begin{cases} 100 \times \exp\left(0.13 - \frac{|SOD - 6|}{15} - 0.12GU\right), & 4 > SOD > 8 \\ 100 \times \exp(-0.12GU), & 2 \leq SOD \leq 6 \end{cases} \quad (4)$$

Where, SOD is the average distance between the head and the inside mesh of the liner. The optimal value of SOD should be greater than zero to ensure thermal control of the helmet and comfort, with the addition of thin foam padding [6]. GU represents the standard deviation of the gap distribution, and is a critical parameter for analyzing the dispersion of the distance distribution. An optimized fit is achieved when the GU approaches zero, indicating a more uniform distribution of the standoff distance. In this paper, the Geomagic Wrap 2017 (3D Systems Inc., USA) was utilized to assess the fit of the helmet by measuring the gap between head and the interior liner.

2.5.2. Evaluation of wear comfort by simulation analysis

To calculate the pressure distribution between the head and the bicycle helmet, evaluating the magnitude of peak contact pressure and the uniformity of pressure distribution, and consequently analyze the comfort of wearing the helmet, we established a finite element model for the head and the helmet. As shown in Fig. 7(a), we employed HYPERMESH software (ALTAIR Inc., USA) to mesh the models of the head and the helmet. Following the definition by Lei et al. [39], the outer layer of the head was divided into four levels: scalp-dense bone-spongy bone-dense bone, with the scalp thickness of 7 mm, and the other three levels having a thickness of 3 mm each. Bicycle helmets are typically composed of a shell made of Acrylonitrile Butadiene Styrene (ABS) and a liner made of Expanded Polystyrene (EPS). We measured the thickness of existing helmet shells and liners on the market, and in this study, we set the thickness of the shell to 4 mm and the liner to 15 mm. The material properties and 3D element types used for all finite element models were consistent with those in the studies by Lei et al. [39] and Han et al. [40], as detailed in Table 1.

We conducted a structural static analysis in ANSYS 3D, applying the following constraints and loads to the model: we constrained the bottom of the neck ($U_x = 0, U_y = 0, U_z = 0$) and applied a gravitational field with a magnitude of $G = 9800 \text{ mm/s}^2$ to the entire model. The schematic representation of these constraints and loads is shown in Fig. 7(b). In the typical production of helmets, the shell and liner are bonded together using adhesive to prevent relative displacement between them. Therefore, in the simulation analysis, we employed the shared-node approach to mesh the interface between the helmet shell and liner [41], and the various components of the head were meshed using the same method. Following the definition by Ellena et al. [29], we specified the contact between the helmet liner and the skin of the head as standard contact, with a friction coefficient of 0.4. All simulations were performed using ANSYS 2022 (ANSYS Inc., USA).

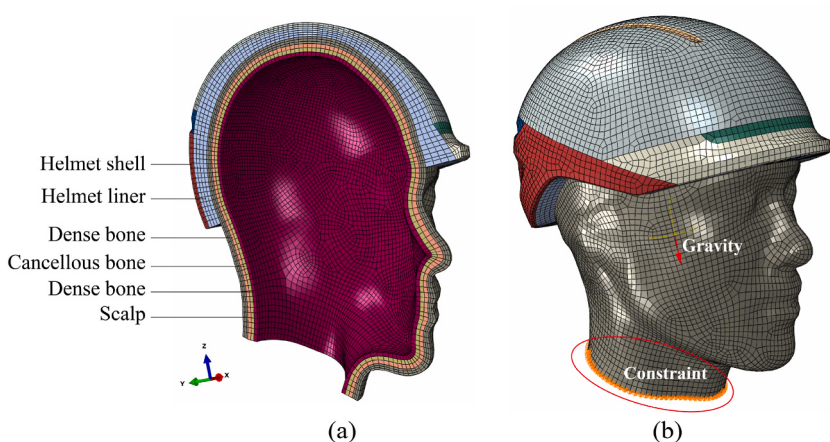


Fig. 7. Model meshing and boundary condition setup. (a) Cross-section of the mesh models for the head and the helmet. (b) Schematic representation of constraints and loads.

Table 1

Mechanical properties and element type of head and bicycle helmet.

Component	Tissue	Density(kg/mm ³)	Young's Modulus (Pa)	Poisson's Ratio	Element type
Head model	Scalp	1.2×10^{-6}	1.67×10^7	0.42	Soild185
Head model	Dense bone	2×10^{-6}	1.8×10^{10}	0.22	Soild185
Head model	Cancellous bone	1.3×10^{-6}	5×10^{10}	0.24	Soild185
Helmet shell	ABS	1.05×10^{-6}	2×10^9	0.30	Soild185
Helmet liner	EPS	7×10^{-8}	2.4×10^7	0.01	Soild185

3. Results and discussion

3.1. Analysis of reconstruction results

According to the data point extraction method described in Section 2.3, we extracted 20 intersecting curves from each 3D head model and transformed them into first-order consisting of 30 data points. Consequently, we obtained a total of 600 data points from each 3D model. Based on these extracted data points, we reconstructed all scanned head models into bicubic Non-Uniform Rational B-Spline (NURBS) surfaces, as shown in Fig. 8(a). Fig. 8(b) represents a schematic of the deviation analysis for the sample after reconstruction, and Fig. 8(c) displays the deviation analysis between all the reconstructed head models and the original head models. The results reveal that the maximum deviation among all the reconstructed surfaces is less than 1.75 mm. These deviation analysis results indicate that the reconstructed 3D head surfaces preserve the information of the original models. Naturally, as the number of extracted data points increases, the reconstruction errors gradually decrease. However, we consider it is essential to balance the reduction in reconstruction error with the computational complexity and duration of the subsequent clustering analysis.

3.2. Analysis of clustering results

It is evident that with fewer clusters for head shape, the production speed and cost of helmets become faster and cheaper. However, it is unavoidable that reducing the number of clusters leads to increased variability within the same cluster of head shapes. The primary goal of any clustering algorithm is to ensure that the differences between samples within each cluster are small. Of course, solely focusing on minimizing differences within clusters and exponentially increasing the number of clusters can render the clustering results statistically insignificant.

Ellena et al. [18] used a distance threshold of 20 mm for corresponding data points between head samples when clustering 3D head shapes of Australians, resulting in the division of the population's head shapes into 4 clusters. Larger distance thresholds between corresponding data points among head shapes lead to fewer clusters. To reduce differences between samples within clusters, we adjusted the distance threshold between corresponding 3D head data points to 15 mm. Both Lacko et al. [31] and Niu et al. [38] have pointed out that Cluster Validity Index (CVI) is a good metric for assessing the clustering quality under different numbers of clusters. It should be emphasized that, according to the calculation formula of CVI (refer to Equations (1)–(3) in Section 2.4.2), increasing the number of clusters does not necessarily result in a reduction of the CVI value. This is because CVI takes into account both intra-cluster differences and inter-cluster differences. This viewpoint has also been demonstrated by Locko et al. [31]. Fig. 9 illustrates the range of CVI values under various cluster numbers. As the number of clusters increases from 3 to 7, the CVI value significantly decreases from 0.921 to 0.175. Indeed, the CVI value is slightly lower at 0.169 when the number of clusters is 11, compared to the CVI value when using 7 clusters. However, the choice of the number of clusters should be based on practical application, taking into account factors

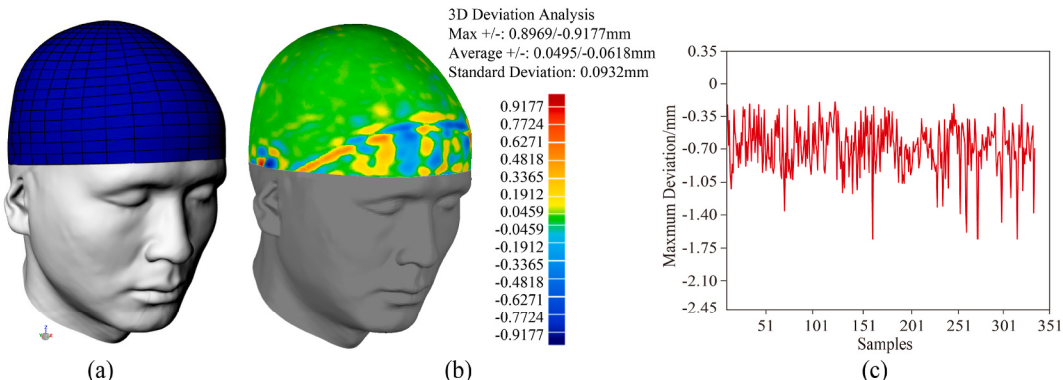


Fig. 8. Results of head model reconstruction and reconstruction deviation analysis. (a) Head reconstructed composed of 600 data points for one sample. (b) Deviation analysis between the reconstructed surface and the original model. (c) Maximum deviations of reconstructed surfaces for 339 samples.

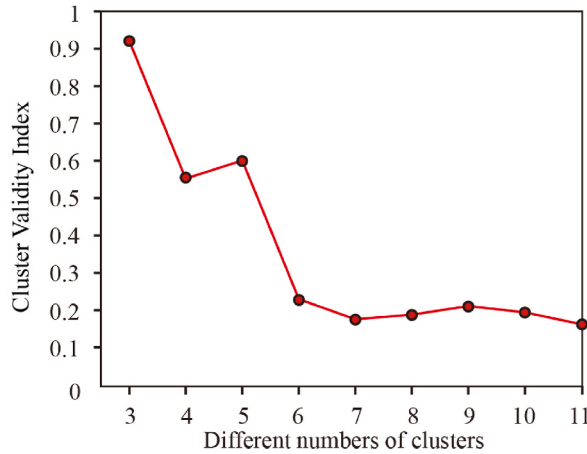


Fig. 9. The distribution of CVI under different numbers of clusters.

such as the feasibility of product manufacturing technology and economic viability. As highlighted by Ellena et al. [18], the reasonable division of product models should meet the following three criteria: the minimal number of clusters, broad coverage of the population, and optimal fit.

The ultimate goal of this paper is to achieve the mass customization of high-fitting bicycle helmets through clustering based on head shape. To determine the optimal number of clusters, we calculated the mean and standard deviation of the Helmet Fit Index (HFI) for different cluster numbers, as shown in Fig. 10. With an increasing number of clusters, the mean HFI exhibits an upward trend. When the number of clusters ranges from 3 to 5, the average HFI is consistently below 70. However, with 6 clusters, the average HFI is 78.08 ± 5.53 , significantly higher than the average HFI for 5 clusters (68.97 ± 6.25). This suggests that one or more head geometry types are distributed among the other clusters. In such a case, increasing the number of clusters is necessary to specifically accommodate individuals with these head types. For cluster numbers ranging from 7 to 11, the average HFI tends to stabilize, with a range of 81.72 ± 5.60 to 83.78 ± 5.14 , indicating a balanced variability within the clusters.

The newly revised GB811-2022 [37], in comparison to the old version GB 811–2010 [42], increased the number of clusters for head shapes from 3 to 5. While the number of clusters in GB 811–2022 is still smaller than the clusters used in our paper, we believe that GB 811–2022 relies solely on head circumference as the clustering criterion and lacks more detailed 3D head data information. As a result, the clustering outcomes may not adequately represent the differences in head shapes.

Therefore, taking into account factors including the number and quality of clusters, helmet fit, and manufacturing considerations, this paper ultimately establishes the number of clusters for head shapes as 7. The medoid surfaces of head for clusters K_1 to K_7 are illustrated in Fig. 11, and detailed clustering results can be found in Table 2. This includes the number and proportion of individuals in each cluster, as well as the key dimensions, such as head circumference, length, and width.

Table 3 provides a comparison between the outcomes of the traditional k -medoids algorithm and the improved k -medoids

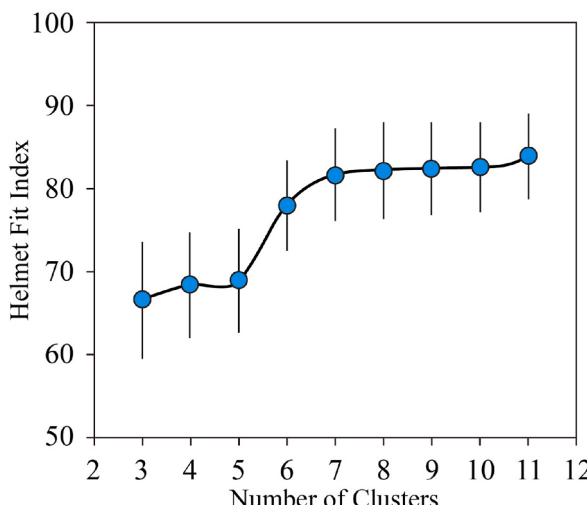


Fig. 10. The distribution of CVI under different numbers of clusters.

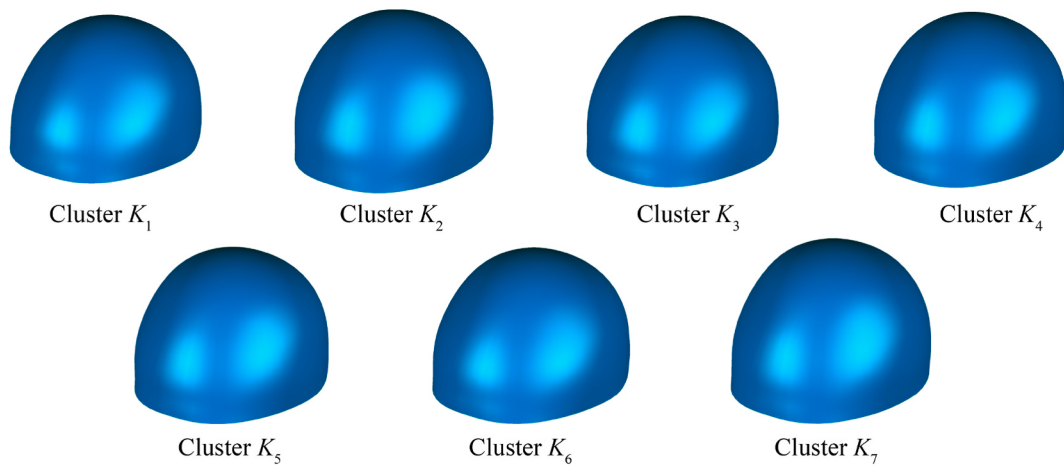


Fig. 11. Medoid surfaces of head shape for clusters K_1 to K_7 .

Table 2

The clustering results and the key dimensions of the medoid surface for head in each cluster.

Clusters	Number of samples	Proportion (%)	Head circumference/mm	Head length/mm	Head width/mm
K_1	25	7.4%	547.20	184.63	164.29
K_2	44	13.0%	572.17	191.20	171.29
K_3	50	14.7%	552.87	186.76	164.54
K_4	35	10.3%	557.06	187.24	167.78
K_5	69	20.4%	551.85	189.73	161.65
K_5	57	16.8%	566.59	195.69	163.29
K_7	59	17.4%	569.34	195.03	166.58

Table 3

Comparison between the traditional and improved k -medoids.

Clustering Algorithms	NPS	Proportion	CVI	Mean/mm	SD/mm
Traditional k -medoids	301	89%	0.167	7.135	3.017
Improved k -medoids	339	100%	0.175	3.751	3.390

Note: NPS-Number of Participating Samples, SD-Standard deviation.

algorithm developed in this study. The comparison is made under identical threshold settings, with the final number of clusters set at 7. The Cluster Validity Index (CVI) for the traditional clustering algorithm is observed to be lower than that of the improved algorithm, possibly due to 38 samples not engaging in the clustering process. Ellena et al. [18] conducted a clustering analysis of the head shapes of the Australian population, comparing the use of traditional hierarchical clustering algorithms with an improved hierarchical

Table 4

The deviation analysis between the medoid surface of the head for each cluster (Unit: mm).

Cluster	Deviation analysis	K_1	K_2	K_3	K_4	K_5	K_6	K_7
K_1	Maximum Distance	Positive	/	19.36	6.20	12.85	12.67	7.71
		Negative	/	-9.67	-6.78	-11.50	-7.73	-0.40
K_2	Maximum Distance	Positive	9.67	/	3.04	0.96	2.10	9.51
		Negative	-19.36	/	-13.64	-8.17	-6.80	-11.91
K_3	Maximum Distance	Positive	6.78	13.64	/	6.73	7.07	7.88
		Negative	-6.20	-3.04	/	-4.83	-1.17	-0.90
K_4	Maximum Distance	Positive	11.50	8.17	4.83	/	5.32	12.63
		Negative	-12.85	-0.96	-6.73	/	-3.75	-7.35
K_5	Maximum Distance	Positive	7.73	6.80	1.17	3.75	/	7.51
		Negative	-12.67	-2.10	-7.07	-5.32	/	-5.19
K_6	Maximum Distance	Positive	0.40	11.91	0.90	7.35	5.19	/
		Negative	-7.71	-9.51	-7.88	-12.63	-7.51	/
K_7	Maximum Distance	Positive	2.77	5.36	0	2.96	0	2.85
		Negative	-17.64	-7.31	-13.71	-12.44	-8.31	-10.18

clustering algorithm. They also noted that when setting the clustering threshold for corresponding vertices between head shapes, the traditional hierarchical clustering algorithm resulted in some samples not participating in the clustering. Calculation of the mean and standard deviation of distances between all corresponding data points within each cluster reveals that the traditional algorithm exhibits greater intra-cluster variations compared to the clustering results of the improved algorithm. As a result, it can be inferred that the improved k -medoids algorithm offers the advantages of increased sample participation and reduced intra-cluster sample variations.

Table 4 presents the results of the deviation analysis between the head shapes of cluster medoids. The results reveal significant differences in the head shapes among the cluster medoids. Among all clusters, Cluster K_1 has the smallest head shape, while Cluster K_2 has the largest head shape, with a maximum positive deviation of 19.36 mm between them. The maximum positive deviation between Clusters K_3 and K_7 is 13.71 mm, with a maximum negative deviation of 0. Between Clusters K_5 and K_7 , the maximum positive deviation is 8.31 mm, with a maximum negative deviation of 0. This indicates that the medoid surface of Cluster K_7 is entirely distinct from those of Clusters K_3 and K_5 .

Fig. 12(a)–(c) illustrate the intersection lines of the medoid surface of each cluster head with the sagittal, coronal, and horizontal planes. As shown in **Table 2**, although the differences in head dimensions, such as head circumference between Clusters K_6 and K_7 , are relatively small, the shape difference between them reaches 10.18 mm. Similarly, the differences in head width between Clusters K_1 and K_7 and between Clusters K_1 and K_5 are relatively small, but the shape differences between them are 17.64 mm and 12.85 mm, respectively. This analysis demonstrates that relying solely on limited head size criteria for head shape clustering often fails to represent the shape differences between heads. Consequently, helmets designed based on such clustering results may not provide a high level of fit. Therefore, when conducting head shape clustering analysis, it is essential to consider the complete 3D shape information of the head.

4. Design and evaluation

4.1. Parametric modeling program for the mass customization of bicycle helmets

The design and modeling process of a bicycle helmet is highly intricate and typically requires experienced designers. To simplify the helmet design and editing process, and to improve the efficiency of mass customization, we have developed a parametric modeling program for bicycle helmets based on the head shape clustering results presented in this paper. This program utilizes GRASSHOPPER software, which is a visual programming plugin for RHINOCEROS software (Robert McNeel & Assoc Inc., Seattle, Washington, USA). The plugin includes various geometric operators, also known as "components," each of which has input and output ports. Designers only need to connect these components based on logical relationships to accomplish the programming. Furthermore, another advantage of this plugin is that it fully records the initial and final parametric modeling process. Designers can simply adjust the initial model or modify the relevant parameters to change the shape of the final generated model.

The helmet parameterized modeling program mainly consists of three modules: helmet liner, shell, and shell surface texture. As shown in **Fig. 13(a)**, the main modeling process of the helmet liner module is as follows: (1) Use the Offset Brep operator to offset the clustered head surface outward by 15 mm (based on the thickness of the existing helmet liner in the market) to obtain the outer surface of the liner; (2) Utilizing the Split Surface operator to trim the inner and outer surfaces of the liner by drawing splitting curves; (3) Employing the Deconstruct Brep operator to extract edge structure lines of the inner and outer sides of the liner,¹ between the inner and outer surfaces using the Loft operator; (4) Merging the inner surface, outer surface, and connecting surfaces to obtain a closed liner solid. The modeling process of the helmet shell module is consistent with the construction steps of the helmet liner module and is shown in **Fig. 13(b)**. **Fig. 13(c)** illustrates the main modeling process of a helmet shell texture module, which includes: (1) Using the Hexagonal operator to create hexagonal array units (the number of hexagons can be adjusted separately in the X, Y, and Z directions); (2) Employing the Evaluate Surface operator to calculate the centers of the hexagonal array units; (3) Using the Remap Numbers operator to set the variation range of the hexagonal array units; (4) Finally, using the Map to Surface operator to map the modified hexagonal array units onto the shell surface.

According to the constructed parametric modeling program, designers no longer need to engage in complex surface modeling. They can quickly obtain different types of bicycle helmets by simply replacing the results of head shape clustering. Additionally, it is possible to swiftly modify the shell texture by adjusting specific parameters. **Fig. 14** illustrates examples of different users virtually wearing bicycle helmets. Currently, the program only includes a basic model of helmet shell and texture modeling procedure. In the future, it will be necessary to establish a library of helmet shell designs and shell textures for the convenience of designers to quickly access and modify shell designs based on the personalized requirements of different users.

4.2. Evaluation of fit for the mass customization bicycle helmet

To assess the fit of mass-customized bicycle helmets based on the clustering results of head shapes, we recruited and collected 3D head models from 6 new participants. These models were then divided into different clusters: participants A-C were assigned to cluster K_2 , while participants D-F were respectively allocated to clusters K_5 , K_6 , and K_3 . As depicted in **Fig. 15**, using the medoid surface of head from cluster K_2 as the helmet liner, we calculated the deviations between this surface and the head surfaces of the 6 new participants. It was evident that the gaps between the heads of participants A, B, and C and the helmet liner were smaller than those of other samples (red areas indicate larger gaps, and green areas indicate smaller gaps). The average deviations and standard deviations between the head shapes of the 6 new samples and the medoid surface of cluster K_2 are presented in **Table 5**. It is important to note that

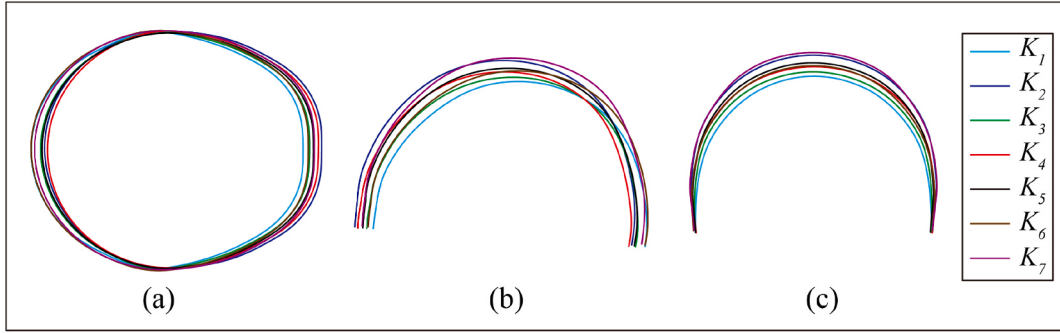


Fig. 12. The intersection lines of the medoid surface of each cluster head. (a) In the sagittal plane. (b) In the coronal plane. (c) In the horizontal plane.

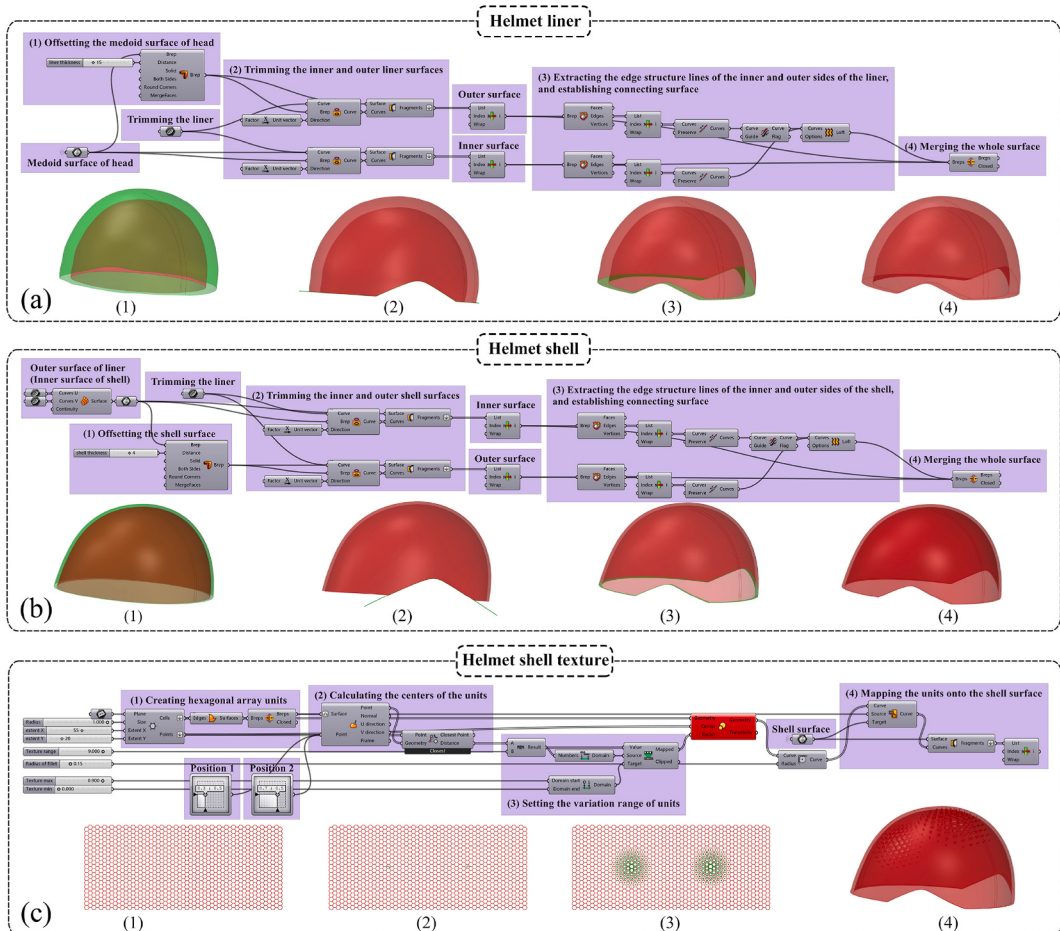


Fig. 13. Parametric modelling program for bicycle helmet. (a) Helmet liner module. (b) Helmet shell module. (c) Helmet shell texture module.

the Helmet Fit Index (HFI) developed by Ellena et al. [17,29] represents the average deviation between head surfaces as Standoff Distance (SOD) and standard deviation as Gap Uniformity (GU). As shown in Table 5, based on the calculation formula of HFI (see Section 2.5.1), we computed the fit scores when the 6 participants wore helmet liner designed according to the medoid surface of head from cluster K_2 . The fit scores for participants A, B, and C were 85.885, 75.238, and 77.484, respectively, markedly higher than the values for participants D, E, and F. This result demonstrates the reliability of the head shape clustering results presented in this study and validates the high fit of helmets designed based on clustering results.

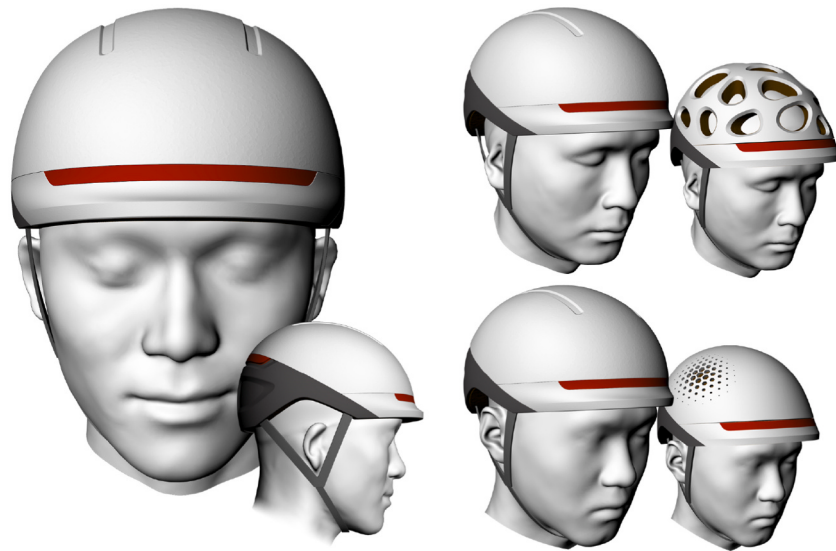


Fig. 14. Examples of different users virtually wearing bicycle helmets.

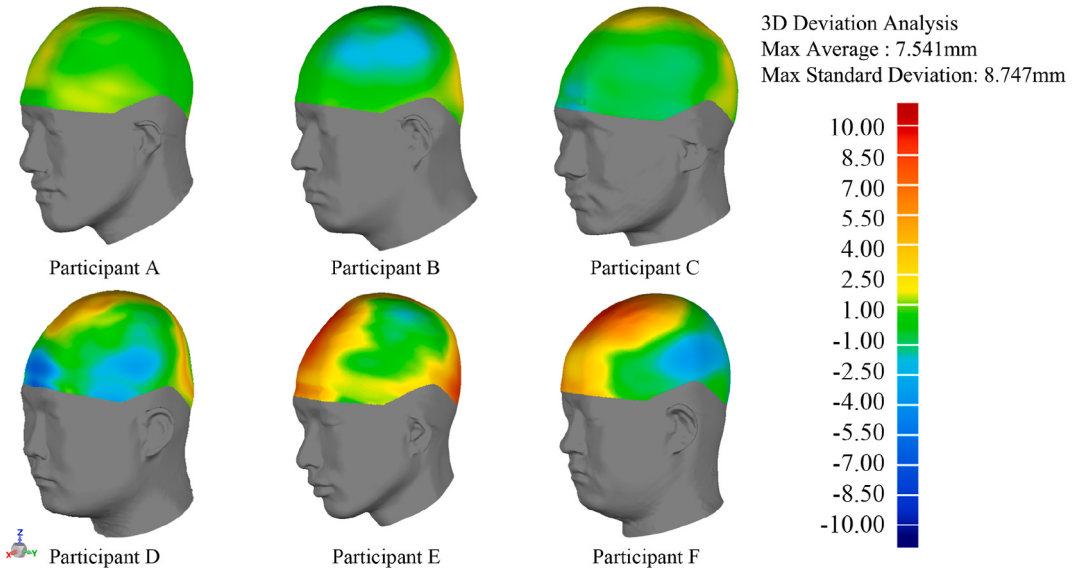


Fig. 15. Deviation analysis between the helmet liner designed by the medoid surface of head from cluster K_2 and the heads of 6 new participants labelled A to F.

Table 5

The Helmet Fit Index for 6 new participants.

Participant	SOD/mm	GU/mm	HFI
A	2.163	1.268	85.885
B	3.551	2.371	75.238
C	1.217	1.663	77.484
D	1.443	3.941	59.847
E	5.748	6.974	43.306
F	7.541	8.747	31.484

4.3. Evaluation of wearing comfort for the mass customization bicycle helmet

According to the method described in section 2.5.2, which includes the meshing of bicycle helmets and the head, setting boundary conditions, etc., we conducted stress simulation analysis on participants wearing helmets designed based on their cluster head shape and helmets designed for non-cluster head shapes. The comfort of the helmets was validated by comparing the magnitude of peak contact pressure and the uniformity of pressure distribution in pressure maps. Fig. 16(a) shows the stress simulation results when participant S_9 , belonging to cluster K_2 , wears a helmet liner designed based on the medoid surface of cluster K_2 's head shape. The stress distribution is uniform, with a maximum pressure of 662.155 Pa. In contrast, when participant S_9 wears a helmet liner designed based on the medoid surface of another cluster, the stress distribution becomes uneven, and the maximum pressure significantly increases to 857.973 Pa, as shown in Fig. 16(b). The results of the simulation analysis emphasize the importance of clustering head shapes and demonstrate that helmet design based on clustering results provides better wearing comfort.

5. Conclusions

This paper presents a novel approach to exploring mass customization design for bicycle helmets, incorporating 3D scanning technology, surface reconstruction techniques, data clustering analysis, and simulation assessment. It is worth noting that we applied an improved k -medoids algorithm to cluster the head data of 339 Chinese males into 7 groups, taking into consideration Cluster Validity Index (CVI), production costs, Helmet Fit Index (HFI), and other indicators. The results of the study indicate: (1) Clustering based solely on limited head dimensions often fails to capture the diversity of head shapes. To enhance the fit and comfort of bicycle helmets in mass customization design, it's essential to consider the overall variation in head shapes. (2) The improved k -medoids algorithm exhibits advantages over the traditional k -medoids algorithm in terms of sample participation rates and minimizing intra-cluster sample differences. It can be anticipated that, compared to the personalized customization design process, the mass customization design method proposed in this paper not only reduces production costs and development cycles but also offers better adaptability and comfort.

Some limitations and future work of this study are as follows.

- We focused solely on the head shapes of Chinese males aged 18–30. However, some references have already indicated age and gender differences in 3D head shapes. Therefore, future research should encompass a broader range of the Chinese population, including males and females under 18 and over 30, to further enhance the inclusivity of clustering results. Additionally, further research efforts should involve the incorporation of facial data to create a comprehensive database of head and facial shapes, providing a basis for the mass customization design of products such as headphones, hearing aids, VR goggles, masks, and more.
- We used the CVI and HFI at various cluster numbers as evaluation metrics to cluster Chinese head shapes into 7 clusters. It's evident that the fewer the clusters, the lower the production costs and the faster the manufacturing speed for helmets. In future research, the setting of point-to-point distance thresholds can be combined with the material properties of helmet liners (if the material is flexible, it can accommodate larger point-to-point differences between head shapes within the same cluster). The setting of the maximum distance threshold will determine the minimum number of clusters.
- Is it possible to modify the existing solid EPS material used for helmet liners in the current market to a porous or lattice structure? While ensuring the safety or rigidity requirements of the helmet, a porous liner offers advantages such as reducing helmet weight and improving breathability. Additionally, a porous liner provides better flexibility, allowing us to decrease the cluster number of head by increasing the set point-to-point distance threshold between head shapes.

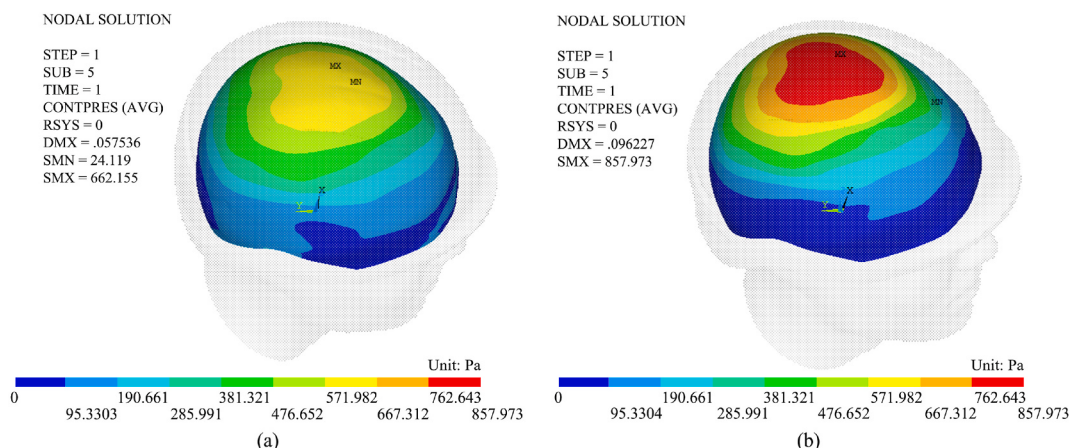


Fig. 16. Stress Simulation Analysis. (a) Stress simulation results when participant S_9 from cluster K_2 wears a helmet liner designed based on the medoid surface of cluster K_2 's head. (b) Stress simulation results when participant S_9 from cluster K_2 wears a helmet liner designed based on the medoid surface of another cluster head.

Ethnics statement

The study was reviewed and approved by the medical ethics committee of the First People's Hospital of Xuzhou, with the approval number: No. xxy11 [2023] 074. All participants provide informed consent to participate in the study.

Data availability statement

Data associated with the study has not been deposited into a publicly available repository and data will be made available on request.

CRediT authorship contribution statement

Zhaohua Zhu: Writing – review & editing, Writing – original draft, Validation, Methodology, Investigation, Funding acquisition, Formal analysis, Data curation, Conceptualization. **Yi Huang:** Writing – review & editing, Writing – original draft, Validation, Supervision, Project administration, Methodology, Investigation, Funding acquisition, Formal analysis, Data curation, Conceptualization. **Wenxuan Ji:** Visualization, Writing – original draft. **Jintuo Zhu:** Writing – review & editing, Writing – original draft, Visualization, Software, Methodology, Formal analysis, Data curation, Conceptualization. **Wenyu Wang:** Writing – review & editing, Writing – original draft, Visualization, Investigation, Data curation.

Declaration of competing interest

The authors declare that they have no known competing financial interests or personal relationships that could have appeared to influence the work reported in this paper.

Acknowledgments

This paper was supported by the National Natural Science Foundation of China (Grant number 52005498); Xuzhou Science and Technology Project (Grant number KC21069); the Fundamental Research Funds for the Central Universities (Grant number 2020SK15); and the Graduate Innovation Program of China University of Mining and Technology (Grant number 2023WLJCRCZL326). We extend our gratitude to the students who willingly participated in this experiment, providing us with invaluable data. Additionally, we would like to express our appreciation to the anonymous reviewers for their insightful comments and helpful suggestions.

References

- [1] N.R. Romanow, B.E. Hagel, J. Williamson, et al., Cyclist head and facial injury risk in relation to helmet fit: a case-control study, *Chronic Dis. Inj. Can.* 34 (2014) 1–7.
- [2] K.T. Thai, A.S. McIntosh, T.Y. Pang, Bicycle helmet size, adjustment, and stability, *Traffic Inj. Prev.* 16 (2015) 268–275.
- [3] F.P. Rivara, S.J. Astley, S.K. Claren, , et al.R.S. Thompson, Fit of bicycle safety helmets and risk of head injuries in children, *Inj. Prev.* 5 (1999) 194–197.
- [4] R. Ball, C. Shu, P.C. Xi, et al., A comparison between Chinese and Caucasian head shapes, *Appl. Ergon.* 41 (2010) 832–839.
- [5] S. Alemany, J. Olaso, B. Nacher, et al., A multidimensional approach to the generation of helmets' design criteria: a preliminary study, *Work* 41 (2012) 4031–4037.
- [6] S. Skals, T. Ellena, A. Subic, et al., Improving fit of bicycle helmet liners using 3D anthropometric data, *Int. J. Ind. Ergon.* 55 (2016) 86–95.
- [7] X.M. Ji, Z.H. Zhu, Z. Gao, et al., Anthropometry and classification of auricular concha for the ergonomic design of earphones, *Hum. Factors Ergon. Manuf.* 28 (2017) 90–99.
- [8] H. Fan, S.H. Yu, J.J. Chu, et al., Anthropometric characteristics and product categorization of Chinese auricle for ergonomic design, *Int. J. Ind. Ergon.* 69 (2019) 118–141.
- [9] K.X. Liu, X.Y. Zeng, J.P. Wang, et al., Parametric design of garment flat based on body dimension, *Int. J. Ind. Ergon.* 65 (2018) 45–69.
- [10] J.F. Jin, Y.C. Yang, F.Y. Zou, et al., Developing an intelligent model for the construction a hip shape recognition system based on 3D body measurement, *Fibers Text. East Eur.* 24 (2016) 110–118.
- [11] Z. Zhuang, C. Shu, P. Xi, et al., Head-and -face shape variations of U. S. civilian workers, *Appl. Ergon.* 44 (2013) 775–784.
- [12] C.H. Chu, S.H. Huang, Design customization of respiratory mask based on 3D face anthropometric data, *Int. J. Precis. Eng. Man.* 16 (2015) 487–494.
- [13] A.M.J.A. Gutierrez, M.D. Galang, R.R. Seva, et al., Designing an improved respirator for automotive painters, *Int. J. Ind. Ergon.* 44 (2014) 131–139.
- [14] Y.C. Lee, M.J. Wang, Taiwanese adult foot shape classification using 3D scanning data, *Ergonomics* 58 (2015) 11–20.
- [15] Y.C. Lee, G. Lin, M.J.J. Wang, Comparing 3D foot scanning with conventional measurement methods, *J. Foot Ankle Res.* 7 (2014) 44–54.
- [16] T. Ellena, S. Skals, A. Subic, et al., 3D digital headform models of Australian cyclists, *Appl. Ergon.* 59 (2017) 11–18.
- [17] T. Ellena, A. Subic, T.Y. Pang, et al., The helmet fit index—an intelligent tool for fit assessment and design customization, *Appl. Ergon.* 55 (2016) 194–207.
- [18] T. Ellena, A. Subic, H. Mustafa, et al., A novel hierarchical clustering algorithm for the analysis of 3D anthropometric data of the human head, *Comput. Aided Des. App.* 15 (2018) 25–33.
- [19] P.W. Wang, J. Yang, Y.A. Hu, et al., Innovative design of a helmet based on reverse engineering and 3D printing, *Alex. Eng. J.* 60 (2021) 3445–3453.
- [20] C.H. Chu, I.J. Wang, J.B. Wang, et al., 3D parametric human face modeling for personalized product design: eyeglasses frame design case, *Adv. Eng. Inf.* 32 (2017) 202–223.
- [21] C.H. Chu, I.J. Wang, Mass customized design of cosmetic masks using three-dimensional parametric human face models constructed from anthropometric data, *J. Comput. Inf. Sci. Eng.* 18 (2018) 1–12.
- [22] C.H. Chu, S.H. Huang, Design customization of respiratory mask based on 3D face anthropometric data, *Int. J. Precis. Eng. Manuf.* 16 (2015) 487–494.
- [23] Z. Li, X. Deng, Y. Lee, et al., Establishment of open web platform based on 3D head model for product adaptability analysis and evaluation, *Heliyon* 8 (2022) e11732.
- [24] J. Zhang, Y. Luximon, P. Shah, et al., Customize my helmet: a novel algorithmic approach based on 3D head prediction, *Comput. Aided Des.* 150 (2022) 103271.

- [25] J. Zhang, Y. Luximon, P. Shah, et al., 3D statistical head modelling for face/head-related product design: a state-of-the-art review, *Comput. Aided Des.* 159 (2023) 103483.
- [26] S.Y. Bake, K. Lee, Parametric human body shape modeling framework for human-centered product design, *Comput. Aided Des.* 44 (2012) 56–67.
- [27] S.Y. Bake, K. Lee, Statistical foot-shape analysis for mass-customization of footwear, *Int. J. Comput. Aided Eng. Technol.* 8 (2016) 80–98.
- [28] C.C. Kuo, M.J. Wang, J.M. Lu, Developing sizing systems using 3D scanning head anthropometric data, *Meas.* 152 (2020) 107264.
- [29] T. Ellena, H. Mustafa, A. Subic, et al., A design framework of the mass customization of custom-fit bicycle helmet models, *Int. J. Ind. Ergon.* 64 (2018) 122–133.
- [30] T.Y. Pang, T.S.T. Lo, T. Ellena, et al., Fit, stability and comfort assessment of custom-fitted bicycle helmet inner liner designs, based on 3D anthropometric data, *Appl. Ergon.* 68 (2018) 240–248.
- [31] D. Lacko, T. Huysmans, J. Vleugels, et al., Product sizing with 3D anthropometry and k-medoids clustering, *Comput. Aided Des.* 91 (2017) 60–74.
- [32] S. Verwulgen, D. Lacko, J. Vleugels, et al., A new data structure and workflow for using 3D anthropometry in the design of wearable products, *Int. J. Ind. Ergon.* 64 (2018) 108–117.
- [33] X.B. Bai, O. Huerta, E. Unver, et al., A parametric product design framework for the development of mass customized head/face (eyewear) products, *Appl. Sci.* 11 (2021) 5382.
- [34] Y. Luximon, R.M. Ball, E.H.C. Chow, A design and evaluation tool using 3D head templates, *Computer-Aided Des. Appl.* 13 (2016) 153–161.
- [35] J. Zhang, H. Iftikhar, P. Shah, et al., Age and sex factors integrated 3D statistical models of adults' heads, *Int. J. Ind. Ergon.* 90 (2022) 103321.
- [36] J. Zhang, F. Fu, X. Shi, et al., Modelling 3D geometric growth patterns and variations of children's heads, *Appl. Ergon.* 108 (2023) 103933.
- [37] National Standardization Administration Committee, G.B., 811-2022 Helmets for Motorcycle and Electric Bicycle Users, China Standards Press, Beijing, 2022.
- [38] J. Niu, Z. Li, G. Salvendy, Multi-resolution shape description and clustering of three-dimensional head data, *Ergonomics* 52 (2009) 251–269.
- [39] Z.P. Lei, J.Z. Yang, Z.Q. Zhuang, Contact pressure study of N95 Filtering face-piece respirators using finite element method, *Computer-Aided Des. Appl.* 7 (2010) 847–861.
- [40] Y. Han, Y. He, L.Y. Li, et al., Ground impact protective performances of different helmets in electric two-wheeler accidents, *J. Vib. Shock* 41 (2022) 55–65.
- [41] N. Mills, A. Gilchrist, Finite-element analysis of bicycle helmet oblique impacts, *Int. J. Impact Eng.* 35 (2008) 1087–1101.
- [42] National Standardization Administration Committee, G.B., 811-2010 Helmets for Motorcycle and Electric Bicycle Users, China Standards Press, Beijing, 2010.